Eur. Phys. J. C (2017) 77:205
DOI 10.1140/epjc/s10052-017-4768-y

THE EUROPEAN PHYSICAL JOURNAL C

Regular Article - Theoretical Physics

Coupling WW, ZZ unitarized amplitudes to $\gamma\gamma$ in the TeV region

Rafael L. Delgado[a], **Antonio Dobado**[b], **Felipe J. Llanes-Estrada**[c]

Departamento de Física Teórica I, Universidad Complutense de Madrid, 28040 Madrid, Spain

Received: 21 December 2016 / Accepted: 19 March 2017 / Published online: 31 March 2017

Abstract We define and calculate helicity partial-wave amplitudes for processes linking the Electroweak Symmetry Breaking Sector (EWSBS) to $\gamma\gamma$, employing (to NLO) the Higgs-EFT (HEFT) extension of the Standard Model and the Equivalence Theorem, while neglecting all particle masses. The resulting amplitudes can be useful in the energy regime (500 GeV−3 TeV). We also deal with their unitarization so that resonances of the EWSBS can simultaneously be described in the $\gamma\gamma$ initial or final states. Our resulting amplitudes satisfy unitarity, perturbatively in α, but for all s values. In this way we improve on the HEFT that fails as interactions become stronger with growing s and we provide a natural framework for the decay of dynamically generated resonances into WW, ZZ and $\gamma\gamma$ pairs.

1 Introduction

1.1 The electroweak symmetry-breaking sector

Electroweak symmetry breaking happens at a scale of $v = 246$ GeV for reasons still unsettled, and the LHC is trying to discern whether the Higgs-like scalar boson found there [1–4] couples to other known particles as dictated by the Standard Model. If the LHC finds new particles or perhaps broad resonances in the TeV region under exploration, it is natural (by the energy scale involved) to guess that they play a role in breaking electroweak symmetry.

Meanwhile, it makes sense to formulate theory in terms of the particles already known to be active in that Electroweak Symmetry breaking sector, namely the new Higgs-like boson h and the longitudinal components of the W and Z electroweak bosons. The resulting, most general, effective field theory that does not assume h to be part of an electroweak doublet, has come to be known as Higgs Effective Field Theory (HEFT) [5–15], and has been built upon the old Higgsless Electroweak Chiral Lagrangian [16–21]. An effort to constrain the parameters of this HEFT from low-energy observables is under way employing LHC data [22]. We adopt the parity-conserving HEFT as our starting point.

To reduce the complexity of the computations and since we are not aiming at a precision description of the WW/hh threshold observables, but rather at the possible resonance region above 500 GeV, we adopt the Equivalence Theorem [23–30]. This is valid for $s \gg M_h^2, M_W^2, M_Z^2 \simeq (100\,\text{GeV})^2$, and it allows one to identify the longitudinal gauge bosons with the pseudo-Goldstone bosons of symmetry breaking ω^a ($a = 1\ldots3$) in their scattering amplitude T. For example one has

$$T(W_L^i W_L^j \to W_L^k W_L^l) = T(\omega^i\omega^j \to \omega^k\omega^l) + \mathcal{O}\left(\frac{M_W}{\sqrt{s}}\right). \tag{1}$$

In our recent work analyzing the EWSBS [31–33] we established that, for any parameter choice separate from the Standard Model, the theory becomes strongly interacting at sufficiently high energy, and resonances may appear. Given the mass gap between the visible EWSBS and those resonances, it makes sense to restrict ourselves to Higgs constant self-couplings that count as order M_h^2, and are thus negligible for $s \gg M_h^2$, so that the Higgs also couples derivatively in our energy interval (as in composite Higgs or dilaton models). Apart from this assumption our discussion remains general. The Lagrangian will be exposed below in Sect. 2.

In principle, HEFT is a usable theory through $E \sim 4\pi v = 3$ TeV, but if new strong interactions and resonances appear in that interval, its applicability region quickly contracts. Even at low energies, truncated HEFT may run into convergence difficulties. These are not alleviated much by increasing the order of the chiral expansion, and on the contrary the number of chiral parameters swiftly increases reducing predictive power. We therefore follow a different strategy to extend

[a] e-mail: rdelgadol@ucm.es
[b] e-mail: dobado@fis.ucm.es
[c] e-mail: fllanes@fis.ucm.es

the low-energy regime by using dispersion relations (DR) compatible with analyticity and unitarity. This approach is extremely useful in the original hadron ChPT [34,35] and we have long advocated it for the SBS of the strongly interaction sector of the SM [36].

Dispersion relations are identities that do not include all dynamical information, but they become much more predictive when the low-energy scattering amplitudes are known (for example from the HEFT). Even so, some model dependence remains in the treatment of amplitude cuts other than that extending for physical s (normally, this applies to the left cut, LC). To constrain it, we employ two different methods, the Inverse Amplitude Method (IAM) and the N/D method. We have detailed both of them in this context in [33] where a complete discussion and references may be found, as well as further unitarization strategies. As will also be exposed later (see Fig. 8), both methods are qualitatively equivalent, but to describe the same resonance they need parameters of the underlying NLO HEFT that are different from each other by 25%.

In the end, the resulting unitarized HEFT (UHEFT) provides an analytical and unitary description of higher-energy dynamics which is essentially unique up to the first resonances. These appear as poles in the second Riemann sheet thanks to the adequate analytical behavior of the amplitudes.

1.2 Coupling to $\gamma\gamma$

The $\gamma\gamma$ channel is by itself not part of the EWSBS, but because photons propagate to the detectors (being reconstructed, e.g. at the electromagnetic calorimeters) they are direct messengers from the collision in the final state. Studies of new particles decaying into two photons have been pursued since the dawn of particle physics [37].

Conversely, photons also provide interesting production mechanisms from the initial state. With slight virtuality they accompany high-energy beam particles: the photon can be thought of as a parton of the proton [38] or the electron in pp and e^-e^+ colliders, respectively. Thus, high-energy colliders can, in a sense, be thought of as photon colliders. The small electromagnetic α lowers the photon flux, but in exchange the initial state is very clean and directly couples to the EWSBS (since the $W^\pm$ are charged particles). For example, the CMS collaboration [39] is already setting bounds to anomalous quartic gauge couplings from an analysis of precisely $\gamma\gamma \to W^+W^-$. Moreover, thanks to Compton backscattering, photon colliders driven by lepton beams are perhaps also a future option [40,41].

Thus, their coupling to the EWSBS is of much interest. Within the context of the HEFT, the perturbative Feynman amplitudes at the one-loop level have already been reported in [42].

In this work we extend the amplitudes to the resonance region. Because unitarity is most easily expressed in terms of partial waves, and because the partial-wave series converges quickly in the "low-energy" domain where HEFT is valid, we have projected the EWSBS as well as the $\gamma\gamma$ over good angular momentum J. In the case of the Goldstone or the Higgs bosons, $L = J$, but when photons are involved, their intrinsic spin is also at play. We have employed the helicity basis to carry out the computations.

While custodial isospin is presumably conserved by the EWSBS (as suggested by LEP), the electromagnetic coupling to the $\gamma\gamma$ state violates its conservation. Still, we can label the partial-wave amplitudes from the initial $\omega\omega$-state isospin in photon–photon production (or the final $\omega\omega$ at a photon collider).

The helicity basis and the corresponding amplitudes are constructed below in Sect. 3. Their partial-wave projections in turn appear in Sect. 4. We show their single- and coupled-channel unitarization in Sect. 5 and some selected numerical examples thereof in Sect. 6; finally, we add a few remarks in Sect. 7.

2 The chiral Lagrangian and its parameterizations

First we quote from Ref. [32] the effective Lagrangian describing the low-energy dynamics of the four light modes: three would-be Goldstone bosons ω^a (WBGBs) and the Higgs-like particle h. This particle content is valid for the energy range $M_h, M_W, M_Z \simeq (100\ \text{GeV})^2 \ll s \ll 4\pi v \simeq 3$ TeV and exhausts the known Electroweak Symmetry Breaking sector. Resonances of these particles' scattering are possible in this interval and we will describe them employing scattering theory based on the effective Lagrangian instead of introducing them as new fields. The starting point to expose the Lagrangian for the ω and h bosons, whose elements are immediately discussed, may be taken as

$$\mathscr{L} = \frac{v^2}{4}\mathscr{F}(h/v)\mathrm{Tr}[(D_\mu U)^\dagger D^\mu U] + \frac{1}{2}\partial_\mu h \partial^\mu h - V(h), \tag{2}$$

where the vacuum constant is $v = 246\,\text{GeV}$, and the arbitrary function

$$\mathscr{F}(h/v) = 1 + 2a\frac{h}{v} + b\left(\frac{h}{v}\right)^2 + \cdots \tag{3}$$

is analytic around vanishing scalar field. The NLO computation for the WBGB sector is quoted in Refs. [31,33]. Note the usage of the spherical parameterization.[1] The extension that includes $\gamma\gamma$ states can be found in Ref. [42], the covariant derivative being

[1] In Ref. [42], we also employed the exponential parametrization of the coset for the $\gamma\gamma$ scattering. While intermediate results (i.e., the Feynman diagrams) are different, the on-shell amplitudes are exactly the same for the two parametrizations.

$$D_\mu U = \frac{i\partial_\mu \omega_i \tau^i}{v} + i\frac{g}{2}W_{\mu,i}\tau^i - i\frac{g'}{2}B_\mu \tau^3 \cdots . \tag{4}$$

Here, the dots represent terms of higher order in (ω^a/v) and whose precise form depends on the particular parametrization of U, and τ_i are Pauli matrices. Finally, we note the definition of charge basis, $\omega^\pm = \frac{\omega^1 \mp i\omega^2}{\sqrt{2}}$, $\omega^0 = \omega^3$. Thus we are using a $SU(2)_L \times U(1)_Y$ gauged non-linear sigma model corresponding to the coset $SU(2)_L \times SU(2)_R/SU(2)_{L+R}$ coupled to the h singlet, where $SU(2)_{L+R}$ is called the custodial group.

Different values of the parameters a and b in Eq. (3) make the Lagrangian density in Eq. (2) represent the low-energy limit of different theoretical models (and the NLO parameters specified shortly will also depend on the underlying theory). For instance, $a^2 = b = 0$ corresponds to the old, Higgsless Electroweak Chiral Lagrangian [16–21] (which had no explicit Higgs field and thus seems ruled out), $a^2 = 1-(v/f)^2, b = 1-2(v/f)^2$ is the low-energy limit of a $SO(5)/SO(4)$ Minimal Composite Higgs Model [43–45], $a^2 = b = (v/f)^2$ can be obtained from dilaton-type models [46,47], and finally $a^2 = b = 1$ represents the SM with a light Higgs (this is the current experimental situation).

There is no strong direct limit over the b parameter, because of the difficulty of measuring a 2-Higgs state. However, an indirect limit arises because of the coupling between the hh decay and the elastic $\omega\omega$ scattering, as we showed in earlier work [48]. The current direct claimed limits over the a parameter, at a confidence level of 2σ (≈95%) are, from CMS [49], $a \in (0.87, 1.14)$; and from ATLAS [50], $a \in (0.96, 1.34)$. Actual experimental analysis may be tracked from [51], which also details the LHC constraints over a number of SM extensions.

2.1 WBGBs scattering and coupling to $\gamma\gamma$

The one-loop computation for $\omega\omega \to \omega\omega$, $\omega\omega \to hh$ and $hh \to hh$ processes was reported in [31,33]. Because of the equivalence theorem regime, $e^2, g^2, g'^2 \ll s/v^2$, the electric charge coupling the photon can be introduced as a perturbation. Thus, the strong physics of the $\omega\omega$ (longitudinal W_L modes) and hh sector dominates over the transverse modes (W_T, γ) and provides the driving force to saturate unitarity. One can then work to leading non-vanishing order when incorporating the transverse modes. The minimum set of counterterms needed to renormalize those scattering amplitudes to one loop is that corresponding to the a_4, a_5, g,[2] d and e parameters (see Refs. [31,33]).

In Ref. [42] we extended the effective NLO Lagrangian for the Higgs and WBGBs [31,33] by including transverse gauge bosons [52] to account for the $\gamma\gamma \to zz$ and $\gamma\gamma \to \omega^+\omega^-$ processes. Concentrating only on $\gamma\gamma$ the effective Lagrangian $\mathscr{L}_2 = \mathscr{L}_2(\omega, h, \gamma)$ becomes

$$\begin{aligned}\mathscr{L}_2 = {} & \frac{1}{2}\partial_\mu h \partial^\mu h + \frac{1}{2}\mathscr{F}(h/v)(2\partial_\mu\omega^+\partial^\mu\omega^- + \partial_\mu\omega^0\partial^\mu\omega^0) \\ & + \frac{1}{2v^2}\mathscr{F}(h/v)(\partial_\mu\omega^+\omega^- + \omega^+\partial_\mu\omega^- + \omega^0\partial_\mu\omega^0)^2 \\ & + ie\mathscr{F}(h/v)A^\mu(\partial_\mu\omega^+\omega^- - \omega^+\partial_\mu\omega^-) \\ & + e^2\mathscr{F}(h/v)A_\mu A^\mu\omega^+\omega^-, \end{aligned} \tag{5}$$

where the photon field is given by $A_\mu = \sin\theta_W W_{\mu,3} + \cos\theta_W B_\mu$ with $\sin\theta_W = g'/\sqrt{g^2+g'^2}$. If the Lagrangian of Eq. (5) is employed at NLO, a counterterm NLO Lagrangian is in principle necessary to guarantee the order by order renormalizability, as customary in EFT. This brings in the additional a_1, a_2, a_3 and c_γ counterterms (see Ref. [42]),

$$\begin{aligned}\mathscr{L}_4 = {} & a_1 \mathrm{Tr}(U\hat{B}_{\mu\nu}U^\dagger\hat{W}^{\mu\nu}) + ia_2\mathrm{Tr}(U\hat{B}_{\mu\nu}U^\dagger[V^\mu, V^\nu]) \\ & - ia_3\mathrm{Tr}(\hat{W}_{\mu\nu}[V^\mu, V^\nu]) - \frac{c_\gamma}{2}\frac{h}{v}e^2A_{\mu\nu}A^{\mu\nu} + \cdots , \end{aligned} \tag{6}$$

where

$$\hat{W}_{\mu\nu} = \partial_\mu\hat{W}_\nu - \partial_\nu\hat{W}_\mu + i[\hat{W}_\mu, \hat{W}_\nu], \tag{7a}$$
$$\hat{B}_{\mu\nu} = \partial_\mu\hat{B}_\nu - \partial_\nu\hat{B}_\mu, \tag{7b}$$
$$\hat{W}_\mu = g\mathbf{W}_\mu\boldsymbol{\tau}/2, \quad \hat{B}_\mu = g'\,B_\mu\tau^3/2, \tag{7c}$$
$$V_\mu = (D_\mu U)U^\dagger, \tag{7d}$$
$$A_{\mu\nu} = \partial_\mu A_\nu - \partial_\nu A_\mu. \tag{7e}$$

Equation (6) can be expanded as

$$\begin{aligned}\mathscr{L}_4 = {} & \frac{e^2a_1}{2v^2}A_{\mu\nu}A^{\mu\nu}(v^2 - 4\omega^+\omega^-) \\ & + \frac{2e(a_2-a_3)}{v^2}A_{\mu\nu}[i(\partial^\nu\omega^+\partial^\mu\omega^- - \partial^\mu\omega^+\partial^\nu\omega^-) \\ & + eA^\mu(\omega^+\partial^\nu\omega^- + \omega^-\partial^\nu\omega^+) \\ & - eA^\nu(\omega^+\partial^\mu\omega^- + \omega^-\partial^\mu\omega^+)] - \frac{c_\gamma}{2}\frac{h}{v}e^2A_{\mu\nu}A^{\mu\nu}. \end{aligned} \tag{8}$$

The chiral counting for the EFT yielding $\omega\omega \to \gamma\gamma$ is compared with that for the elastic $\omega\omega \to \omega\omega$ process in Fig. 1.

Current (2σ) bounds on those NLO parameters are $c_\gamma \in (\frac{-1}{16\pi^2}, \frac{0.5}{16\pi^2})$ [12]; $a_1 < 10^{-3}$, $a_2 \in (-0.26, 0.26)$ and $a_3 \in (-0.1, 0.04)$ [53]. It is practical to quote these bounds for the a_i in terms of the only combination that will be needed in this work which is (conservatively adding them) $(a_1 - a_2 + a_3) \in (-0.36, 0.3)$. We will employ these limits when we illustrate the parameter dependence later on in Sect. 6.

[2] Not to be confused with the $SU(2)_L$ gauge coupling.

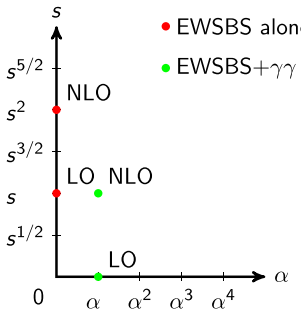

Fig. 1 A sensible counting for $\omega\omega \to \gamma\gamma$, in the energy region around $\mathcal{O}(0.5\ \text{TeV})$ of interest for the LHC, is to take α_{EM} and $s/(4\pi v)^2$ as small quantities with α_{EM} (of smaller size) only to first order. The resulting counting (*green dots*) is compared with that for the purely Goldstone boson processes $\omega\omega \to \omega\omega$ (*red dots*)

3 Matrix elements for $\gamma\gamma$ to $\omega\omega$ and hh scattering at NLO

The one-loop perturbative amplitudes for the production of $\gamma\gamma$ from the EWSBS can be read off (by time reversal invariance) from those for $\gamma\gamma \to \omega\omega$ scattering, computed in [42]. Both $\gamma\gamma \to zz$ and $\gamma\gamma \to \omega^+\omega^-$ amplitudes were there decomposed as

$$\mathscr{M}_{\lambda_1\lambda_2} = iT = ie^2\left(\varepsilon_1^\mu \varepsilon_2^\nu T^{(1)}_{\mu\nu}\right) A + ie^2\left(\varepsilon_1^\mu \varepsilon_2^\nu T^{(2)}_{\mu\nu}\right) B, \quad (9)$$

with Lorentz structures

$$\left(\varepsilon_1^\mu \varepsilon_2^\nu T^{(1)}_{\mu\nu}\right) = \frac{s}{2}(\varepsilon_1\varepsilon_2) - (\varepsilon_1 k_2)(\varepsilon_2 k_1), \quad (10a)$$

$$\left(\varepsilon_1^\mu \varepsilon_2^\nu T^{(2)}_{\mu\nu}\right) = 2s(\varepsilon_1\Delta)(\varepsilon_2\Delta) - (t-u)^2(\varepsilon_1\varepsilon_2) - 2(t-u)[(\varepsilon_1\Delta)(\varepsilon_2 k_1) - (\varepsilon_1 k_2)(\varepsilon_2\Delta)]. \quad (10b)$$

Here, $e = \sqrt{\alpha/4\pi} \approx 0.303$ is the electric charge; $\varepsilon_i(\lambda_i)$, $\lambda_i = \pm 1$ and k_i are the polarization state vector, the helicity and the 4-momentum of each photon with $i = 1, 2$; p_i, the 4-momenta of the Gauge boson ($i = 1, 2$); and $\Delta^\mu = p_1^\mu - p_2^\mu$.

The $\gamma\gamma \to zz$ process, at order $\mathcal{O}(e^2)$ and leading chiral order, vanishes because the Z is a neutral particle,

$$\mathscr{M}(\gamma\gamma \to zz)_{\text{LO}} = 0. \quad (11)$$

The NLO contribution depends on c_γ,

$$A(\gamma\gamma \to zz)_{\text{NLO}} = \frac{2ac_\gamma^r}{v^2} + \frac{a^2-1}{4\pi^2 v^2} \equiv A_N, \quad (12a)$$

$$B(\gamma\gamma \to zz)_{\text{NLO}} = 0. \quad (12b)$$

For $\gamma\gamma \to \omega^+\omega^-$ (the only other process allowed by charge conservation), at order $\mathcal{O}(e^2)$,

$$A(\gamma\gamma \to \omega^+\omega^-)_{\text{LO}} = 2sB(\gamma\gamma \to \omega^+\omega^-)_{\text{LO}} = -\frac{1}{t} - \frac{1}{u}, \quad (13)$$

whereas, at NLO in the counting of Fig. 1,

$$A(\gamma\gamma \to \omega^+\omega^-)_{\text{NLO}} = \frac{8(a_1^r - a_2^r + a_3^r)}{v^2} + \frac{2ac_\gamma^r}{v^2} + \frac{a^2-1}{8\pi^2 v^2} \equiv A_C, \quad (14a)$$

$$B(\gamma\gamma \to \omega^+\omega^-)_{\text{NLO}} = 0. \quad (14b)$$

Interestingly, in dimensional regularization all UV divergences cancel after some algebra, so that no renormalization is required and

$$c_\gamma^r = c_\gamma, \quad (15a)$$

$$a_1^r - a_2^r + a_3^r = a_1 - a_2 + a_3. \quad (15b)$$

Thus this particular combination of the chiral parameters a_1, a_2 and a_3 turns out to be finite and the corresponding renormalized one does not depend on any renormalization scale μ.

We assign momenta and polarization vectors $\varepsilon_i(\pm)$ to the initial-state vector and final-state scalar bosons as

$$\{\gamma[\varepsilon_1(\pm), k_1], \gamma[\varepsilon_2(\pm), k_2]\} \to \{(\omega/h)[p_1], (\omega/h)[p_2]\}, \quad (16)$$

In the cm frame we may choose the coordinate axes such that

$$k_1 = (E, 0, 0, E) \quad k_2 = (E, 0, 0, -E), \quad (17a)$$

$$p_1 = (E, \mathbf{p}) \quad p_2 = (E, -\mathbf{p}) \quad \Delta = p_1 - p_2, \quad (17b)$$

$$\mathbf{p} = (p_x, p_y, p_z) = E(\sin\theta\cos\varphi, \sin\theta\sin\varphi, \cos\theta). \quad (17c)$$

Because in the cm $\mathbf{k}_1 \parallel \mathbf{k}_2$, the 4-dimensional polarization states $\varepsilon_i(\pm)$ are perpendicular to both, $\varepsilon_i(\pm)\cdot k_j = 0$. This simplifies Eqs. (10a) and (10b) to

$$\left(\varepsilon_1^\mu \cdot \varepsilon_2^\nu T^{(1)}_{\mu\nu}\right) = \frac{s}{2}\varepsilon_1\cdot\varepsilon_2, \quad (18)$$

and (since the WBGBs are massless, $(t-u)^2 = s^2\cos^2\theta$),

$$\left(\varepsilon_1^\mu \cdot \varepsilon_2^\nu T^{(2)}_{\mu\nu}\right) = 2s(\varepsilon_1\cdot\Delta)(\varepsilon_2\cdot\Delta) - s^2(\cos\theta)^2(\varepsilon_1\cdot\varepsilon_2). \quad (19)$$

The product $(\varepsilon_1\cdot\varepsilon_2)$ appearing satisfies a modified orthogonality relation because the momenta of the two photons are opposite; choosing

$$\varepsilon_1(\pm) = \frac{1}{\sqrt{2}}(0, \mp 1, -i, 0), \quad (20a)$$

$$\varepsilon_2(\pm) = \frac{1}{\sqrt{2}}(0, \mp 1, i, 0), \quad (20b)$$

we have $\varepsilon_1(+)\cdot\varepsilon_2(-) = \varepsilon_1(-)\cdot\varepsilon_2(+) = 0$ and $\varepsilon_1(+)\cdot\varepsilon_2(+) = \varepsilon_1(-)\cdot\varepsilon_2(-) = -1$. Thus, the Lorentz structures needed for Eqs. (18) and (19) become those shown on Table 1.

The structure of Table 1 is remarkable. First, the amplitudes with equal photon helicities, T^{++} and T^{--}, come in the combination $-\frac{s}{2}A + s^2 B$. But, due to Eq. (13), this just cancels the LO contribution, and with it Rutherford's $1/t$

Table 1 Lorentz structures $\varepsilon_1^\mu \cdot \varepsilon_2^\nu T_{\mu\nu}^{(1)}$ and $\varepsilon_1^\mu \cdot \varepsilon_2^\nu T_{\mu\nu}^{(2)}$ (Eqs. (18) and (19)). All are invariant under $\theta \to \pi - \theta$, that is, t–u exchange, a consequence of Bose symmetry that guarantees $\mathscr{M}(\gamma\gamma \to \omega^+\omega^-)_{\text{LO,NLO}} = \mathscr{M}(\gamma\gamma \to \omega^-\omega^+)_{\text{LO,NLO}}$

$(\lambda_1\lambda_2)$	$(++)$	$(+-)$	$(-+)$	$(--)$
$[\varepsilon_1^\mu(\lambda_1) \cdot \varepsilon_2^\nu(\lambda_2)]T_{\mu\nu}^{(1)}$	$-s/2$	0	0	$-s/2$
$[\varepsilon_1^\mu(\lambda_1) \cdot \varepsilon_2^\nu(\lambda_2)]T_{\mu\nu}^{(2)}$	s^2	$-s^2(\sin\theta)^2 e^{2i\varphi}$	$-s^2(\sin\theta)^2 e^{-2i\varphi}$	s^2

collinear divergence (and the exchanged one in $1/u$). There is no photon–photon annihilation with equal helicity into the Goldstone bosons at LO. Second, the opposite-helicity combinations T^{+-} and T^{-+} are non-vanishing at LO, but again Table 1 assigns a kinematic factor $\sin^2\theta$, which just cancels the angular dependence from the t- and u-channel ω exchange diagrams, and thus once more the collinear divergences drop out. Therefore, polar angular integrals may easily be computed and partial-wave amplitudes to be introduced in Sect. 4 are well defined for all helicity combinations.

Since we formulate unitarity of the EWSBS in terms of custodial $SU(2)_{L+R}$ isospin partial waves, we define the $\omega\omega$ states in the isospin basis $|I, I_3\rangle$ by using the appropriate Clebsch–Gordan coefficients and the standard phase conventions [54], with $|1,1\rangle \equiv -\omega^+$, $|1,0\rangle \equiv \omega^0$, $|1,-1\rangle \equiv \omega^-$. Because of charge conservation, $\gamma\gamma$ only couples to states where the total electric charge I_3 vanishes. Hence, our isospin basis for the relevant $\omega\omega$ states is

$$|0,0\rangle = -\frac{1}{\sqrt{3}}\left(|\omega^+\omega^-\rangle + |\omega^-\omega^+\rangle + |zz\rangle\right), \tag{21a}$$

$$|2,0\rangle = \frac{1}{\sqrt{6}}\left(2|zz\rangle - |\omega^+\omega^-\rangle - |\omega^-\omega^+\rangle\right). \tag{21b}$$

To shorten notation in the next paragraphs, we use the letters N and C (for "neutral" and "charged", respectively) to indicate, the zz and $\omega^+\omega^-$ final states (in the charge basis), as defined in Eqs. (12) and (14). We further shorten $T_I^{\lambda_1\lambda_2} \equiv \langle I, 0|T|\lambda_1\lambda_2\rangle$; explicitly, because of Eq. (21),

$$T_0^{\lambda_1\lambda_2} = -\frac{1}{\sqrt{3}}\left(2T_C^{\lambda_1\lambda_2} + T_N^{\lambda_1\lambda_2}\right), \tag{22a}$$

$$T_2^{\lambda_1\lambda_2} = \frac{2}{\sqrt{6}}\left(T_N^{\lambda_1\lambda_2} - T_C^{\lambda_1\lambda_2}\right). \tag{22b}$$

Taking into account Eq. (12a) through (14b), we find

$$T_0^{++} = T_0^{--} = \frac{e^2 s}{2\sqrt{3}}\left(2A_C + A_N\right), \tag{23a}$$

$$T_2^{++} = T_2^{--} = \frac{e^2 s}{\sqrt{6}}\left(A_C - A_N\right), \tag{23b}$$

$$T_0^{+-} = (T_0^{-+})^* = \frac{4e^2}{\sqrt{3}}e^{2i\varphi}, \tag{23c}$$

$$T_2^{+-} = (T_2^{-+})^* = \frac{4e^2}{\sqrt{6}}e^{2i\varphi}. \tag{23d}$$

We now turn to the isosinglet scattering amplitude with two Higgses, and we obtain

$$R(\gamma\gamma \to hh) = -\frac{e^2}{8\pi^2 v^2}(a^2 - b)(\varepsilon_1 \cdot \varepsilon_2). \tag{24}$$

This is an NLO scattering amplitude as the LO one vanishes. It is proportional to $(a^2 - b)$ and thus to the LO crossed-channel $\omega\omega \to hh$. If BSM physics does not couple hh and $\omega\omega$, then, because hh has no charge, it decouples from $\gamma\gamma$ too.

With the polarization vectors of Eq. (20), Eq. (24) becomes

$$R(\gamma\gamma \to hh) = \frac{e^2}{8\pi^2 v^2}(a^2 - b)\delta_{\lambda_1,\lambda_2} \tag{25}$$

as the final $|hh\rangle$ state is an isospin singlet; or explicitly,

$$\begin{aligned} R_0^{++} &= R_0^{--} = \langle hh|T(\gamma\gamma \to hh)|{++}\rangle \\ &= \frac{e^2}{8\pi^2 v^2}(a^2 - b). \end{aligned} \tag{26}$$

4 Scattering partial waves with $\gamma\gamma$ states

In order to unitarize the $\gamma\gamma \to \omega\omega$ scattering amplitudes, we will use the partial-wave decomposition

$$P_{IJ}^{\lambda_1\lambda_2} = \frac{1}{128\pi^2}\sqrt{\frac{4\pi}{2J+1}}\int \mathrm{d}\Omega\, T_I^{\lambda_1\lambda_2}(s,\Omega)Y_{J,\Lambda}(\Omega), \tag{27}$$

where $\Lambda = \lambda_1 - \lambda_2$, and whose inverse is

$$T_I^{\lambda_1\lambda_2}(s,\Omega) = 128\pi^2 \sum_J \sqrt{\frac{2J+1}{4\pi}} P_{IJ}^{\lambda_1\lambda_2} Y_{J,\Lambda}(\Omega). \tag{28}$$

Note that, because of Bose symmetry, our 2-photon helicity state $|\lambda_1\lambda_2\rangle$ is, indeed, defined as

$$|\lambda_1\lambda_2\rangle = \frac{1}{N}\left(|+k\hat{e}_z, \lambda_1; -k\hat{e}_z, \lambda_2\rangle + |-k\hat{e}_z, \lambda_2; +k\hat{e}_z, \lambda_1\rangle\right). \tag{29}$$

Hence, the parity operator $\mathscr{P}$ acts according to [55–57]

$$\mathscr{P}|{\pm\pm}\rangle = |{\mp\mp}\rangle, \quad \mathscr{P}|{\pm\mp}\rangle = |{\pm\mp}\rangle. \tag{30}$$

This allows us to define a basis for the 2-photon states with three positive parity states,

$$\frac{1}{\sqrt{2}}(|++\rangle + |--\rangle), \quad |+-\rangle, \quad |-+\rangle, \tag{31}$$

and only one negative parity state,

$$\frac{1}{\sqrt{2}}(|++\rangle - |--\rangle), \tag{32}$$

which decouples from the EWSBS because of parity conservation. For $J = 0$, our scattering amplitude only couples to the positive parity state $(|++\rangle + |--\rangle)/\sqrt{2}$. Thus, let us introduce the notation

$$P_{I0} \equiv \frac{1}{\sqrt{2}}\left(P_{I0}^{++} + P_{I0}^{--}\right) = \sqrt{2}P_{I0}^{++} = \sqrt{2}P_{I0}^{--}. \tag{33}$$

For $J = 2$, the only non-vanishing contributions come from P_{I2}^{+-} ($\Lambda = +2$) and P_{I2}^{-+} ($\Lambda = -2$). The amplitudes with $\Lambda = 0$ vanish (see Eq. (23)). Hence, let us define

$$P_{I2} \equiv P_{I2}^{+-} = P_{I2}^{-+}. \tag{34}$$

With these definitions, the lowest non-vanishing-order (denoted with a (0) superindex) $\gamma\gamma$ partial waves are

$$P_{00}^{(0)} = \frac{e^2 s}{32\pi\sqrt{6}}(2A_C + A_N) \quad P_{02}^{(0)} = \frac{e^2}{24\pi\sqrt{2}}, \tag{35a}$$

$$P_{20}^{(0)} = \frac{e^2 s}{32\pi\sqrt{3}}(A_C - A_N) \quad P_{22}^{(0)} = \frac{e^2}{48\pi}. \tag{35b}$$

Here, the $J = 0$ partial waves are NLO while the $J = 2$ ones are LO.

The hh final state is an isospin singlet, and it only couples with $J = 0$ and positive parity states (see Eq. (26)). Thus, the corresponding partial waves are

$$R_I^{(0)} \equiv \frac{1}{\sqrt{2}}\left(R_{I0}^{++} + R_{I0}^{--}\right) = \sqrt{2}R_{I0}^{++}. \tag{36}$$

Hence,

$$R_0^{(0)} = \frac{e^2}{128\sqrt{2}\pi^3 v^2}(a^2 - b). \tag{37}$$

Finally, let us introduce the fine structure constant $\alpha = e^2/4\pi$ on Eqs. (35a) and (35b), so that the P_{IJ} and R_0 to NLO turn into

$$P_{00}^{(0)} = \frac{\alpha s}{8\sqrt{6}}(2A_C + A_N) \quad P_{02}^{(0)} = \frac{\alpha}{6\sqrt{2}}, \tag{38a}$$

$$P_{20}^{(0)} = \frac{\alpha s}{8\sqrt{3}}(A_C - A_N) \quad P_{22}^{(0)} = \frac{\alpha}{12}, \tag{38b}$$

$$R_0^{(0)} = \frac{\alpha}{32\sqrt{2}\pi^2 v^2}(a^2 - b). \tag{38c}$$

These last equations are the ones to be used in practice, with A_c and A_N taken from Eqs. (12) and (14).

5 Unitarity requires $\omega\omega$ resonances to be visible in $\gamma\gamma$

Unitarization of the elastic $\omega\omega$ and the cross-channel $\omega\omega \to hh$ cases has been extensively reported in our earlier work [32,33,48] and that of other groups [58–61] and will not be repeated here. In this section, we will extend the discussion therein to include the $\gamma\gamma$ channel,

$$\gamma\gamma \longleftrightarrow \{\omega\omega, hh\}. \tag{39}$$

The perturbative partial-wave amplitudes involving two photons have been given in Sect. 3 and their partial-wave projections in Sect. 4 so we have all the necessary ingredients from perturbation theory at hand. As the photon is a spin-1 massless boson, Landau–Yang's theorem forbids the partial wave with $J = 1$. Thus, to NLO in the effective theory, the possible angular momenta are $J = 0,\ 2$.

The $\omega\omega$ partial waves decouple from the hh channel for $a^2 = b$, (see Eq. (37)). In keeping the more general $a^2 \neq b$ situation, the reaction matrix includes an inelastic $\gamma\gamma \to hh$ coupling and is not block diagonal.

Because the electromagnetic interaction violates custodial isospin conservation (each ω boson has a different electric charge), the $\gamma\gamma$ state couples to both $I = 0$ and $I = 2$ (unlike hh, which is a singlet $|0, 0\rangle = |hh\rangle$). Though each channel has its own separate strong dynamics, they both provide probability flow into the $\gamma\gamma$ state as dictated by the corresponding Clebsch–Gordan coefficients.

5.1 $\gamma\gamma$ scattering with hh channel decoupled

To start with, let us decouple the hh channel by setting $a^2 = b$ (and other parameters coupling $\omega\omega$ and hh in our earlier work, $d = e = 0$). Then the amplitude matrix is three by three (we specify the $I = 0, 2$ isospin index to make the three-channel nature of the matrix manifest; for each of them, the angular momentum index J can also take the values 0 or 2). It can be given as

$$F(s) = \begin{pmatrix} A_{0J}(s) & 0 & P_{0J}(s) \\ 0 & A_{2J}(s) & P_{2J}(s) \\ P_{0J}(s) & P_{2J}(s) & 0 \end{pmatrix} + \mathcal{O}(\alpha^2), \tag{40}$$

where $A_{IJ}(s)$ are the (isospin conserving) elastic partial waves $\omega\omega \to \omega\omega$ (see [31,33] for the exact definition and main properties) and $P_{IJ}(s)$, the partial-wave projected $\gamma\gamma \to \omega\omega$ amplitudes. Note that we consider only the leading order in the electromagnetic coupling α. Hence, $\langle\gamma\gamma|F^{(0)}|\gamma\gamma\rangle \simeq 0$.

The unitarity condition on a coupled-channel problem is

$$\mathrm{Im}\, F(s) = F(s)F(s)^\dagger \tag{41}$$

on the right cut (RC). Because the interactions among Goldstone bosons grow with s and become strong, a unitarization scheme is mandatory to have a sensible amplitude [34,35].

On the other hand, since α remains small, it can be considered at leading order so that Eq. (41) will be satisfied to all orders in s but only to LO in α, with no appreciable error. Imposing the unitarity condition to Eq. (40) and working to LO in α returns

$$\text{Im}\, A_{IJ} = |A_{IJ}|^2, \tag{42a}$$
$$\text{Im}\, P_{IJ} = P_{IJ} A_{IJ}^*. \tag{42b}$$

The reader can appreciate that the second of these equations is linear in P_{I0} and does not involve the $\gamma\gamma \to \gamma\gamma$ kernel in the LO approximation in the α expansion. The structure of Eq. (42) allows one to sequentially solve the unitarity equation for elastic $\omega\omega$ scattering and then use it to unitarize the final state $\omega\omega \to \gamma\gamma$ amplitude. According to Ref. [33], the elastic $\omega\omega \to \omega\omega$ amplitude admits a chiral expansion

$$A(s) = A^{(0)}(s) + A^{(1)}(s) + \mathcal{O}(s^3), \tag{43}$$

where

$$A^{(0)}(s) = Ks, \tag{44a}$$
$$A^{(1)}(s) = \left(B(\mu) + D \log \frac{s}{\mu^2} + E \log \frac{-s}{\mu^2} \right) s^2. \tag{44b}$$

All the coefficients K (Eq. (44a)), $B(\mu)$, D and E (Eq. (44b)) are given in Ref. [33] for each partial wave.

The unitarization of the scalar $\omega\omega \to \omega\omega$ ($J = 0$) partial wave is beautifully achieved by the elastic IAM method, constructed from the first two orders of the perturbative expansion $A = A^{(0)} + A^{(1)} + \ldots$,

$$\tilde{A}(s) = \frac{A^{(0)}(s)}{1 - \frac{A^{(1)}(s)}{A^{(0)}(s)}}. \tag{45}$$

There is more to this simple equation than meets the eye. It has the correct analytic structure in the complex s plane, allowing for resonances in the second Riemann sheet below the RC, where it satisfies elastic unitarity. At low $\sqrt{s}$ it matches the chiral expansion as can be seen by reexpanding it. And since its derivation follows from a fully prescribed dispersion relation, it can be written down to higher orders (should e.g. the NNLO chiral amplitude become known) without ambiguity.

Turning to the channel-linking P amplitudes, the second of Eq. (42) is the statement of Watson's theorem, which sets its phase to that of $\omega\omega$ rescattering. A solution strategy is, as in the case of $A(s)$, to write a dispersion relation for the auxiliary "inverse" function $w'(s) = P^{(0)2}/P(s)$ with contributions coming from the RC (right cut), the LC (left cut) and the infinite circle. To solve this dispersion relation the simplest ansatz for $w'(s)$ is $w'(s) = f(s)w(s)$ where $f(s)$ is real for real s and $w(s) = (A^{(0)}(s))/A(s)$. The low-energy behavior of $P(s)$ dictates, upon matching to it, $f(s) = P^{(0)}/A^{(0)}(s)$. Then we can use the IAM result for $w(s)$ and obtain

$$\tilde{P} = \frac{P^{(0)}}{A^{(0)}} \tilde{A}. \tag{46}$$

On the RC the imaginary part of $\tilde{P}$ is

$$\text{Im}\, \tilde{P} = \frac{P^{(0)}}{A^{(0)}} \text{Im}\, \tilde{A} = \frac{P^{(0)}}{A^{(0)}} |\tilde{A}|^2 = \tilde{P} \tilde{A}^*, \tag{47}$$

as required by exact unitarity. The $\tilde{P}(s)$ function has the necessary analytical structure (RC and LC) and the appropriate low-energy limit $\tilde{P}(s) \simeq P^{(0)} + \cdots$. Moreover, it features the same poles in the second Riemann sheet as $\tilde{A}(s)$ does, which represent dynamical resonances also in agreement with unitarity and analyticity. Thus, our unitarized $\gamma\gamma \to \omega\omega$ matrix element will be

$$\tilde{P}_{I0} = \frac{P_{I0}^{(0)}}{1 - \frac{A_{I0}^{(1)}}{A_{I0}^{(0)}}}, \quad I = 0, 2. \tag{48}$$

The computation of the $P_{I0}^{(0)}$ partial waves for the $\gamma\gamma \to \omega\omega$ can be found in Sect. 4.

Now we deal with the tensor $J = 2$ channel: note here that the P_{I2} are constant. Also, we have a vanishing LO elastic $\omega\omega$ scattering amplitude $A_{I2} = K_{I2} s$ because $K_{I2} = 0$. And due to $A^{(0)} = 0$, the IAM unitarization method in Eq. (45) cannot be applied. Hence, the N/D method will be used here. In the scalar channel we know that both methods (as well as others), provide very similar solutions to the IAM (see Ref. [33]). A quick, algebraic way to construct an approximation to the N/D system of dispersion relations that satisfies elastic unitarity for all s and has the right analytic properties, having only at hand one order of perturbation theory (here, the NLO) is

$$\tilde{A} = A^{\text{N/D}} = \frac{A_L(s)}{1 + \frac{1}{2} g(s) A_L(-s)}, \tag{49}$$

where

$$g(s) = \frac{1}{\pi} \left(\frac{B(\mu)}{D} + \log \frac{-s}{\mu^2} \right), \tag{50a}$$
$$A_L(s) = \left(\frac{B(\mu)}{D} + \log \frac{s}{\mu^2} \right) D s^2 = \pi g(-s) D s^2. \tag{50b}$$

The B and D which appear in Eq. (50b) are the same that those in Eq. (44b). Note that, by means of perturbative unitarity, $K = 0 \implies E = 0$, thus simplifying the full N/D expression of Ref. [33].

Once the $J = 2$ elastic $\omega\omega$ waves have been unitarized, it is easy to satisfy the second of Eq. (42), following a logic similar to that of the IAM, by

$$\tilde{P}_{I2} = \frac{P_{I2}^{(0)}}{A_{\text{L},I2}} A_{I2}^{\text{N/D}}, \quad I = 0, 2. \tag{51}$$

For $J = 0$ we need to use the full expressions of [33].

5.2 Coupled $\gamma\gamma \longleftrightarrow (\omega\omega, hh)$ scattering

We now proceed to an analysis of the coupled $\omega\omega$ (that is, $W_L W_L$ and $Z_L Z_L$ as per the ET) and hh channels feeding the $\gamma\gamma$ state. Because the electromagnetic interaction violates isospin conservation, the reaction matrix must include both $I = 0, 2$ subchannels of the $\omega\omega$ system, and it is thus of dimension four. Assuming weak isospin conservation in the Goldstone dynamics, which puts zeros in row three and column three, and to order α, which makes the (4, 4) element vanish, it is

$$F = \begin{pmatrix} A_{0J} & M_J & 0 & P_{0J} \\ M_J & T_J & 0 & R_J \\ 0 & 0 & A_{2J} & P_{2J} \\ P_{0J} & R_J & P_{2J} & 0 \end{pmatrix} + \mathcal{O}(\alpha^2). \tag{52}$$

Here again, $A_{IJ}(s)$ are the partial waves $\omega\omega \to \omega\omega$; $M_J(s)$, the $\omega\omega \to hh$ partial wave; $T_J(s)$, the elastic $hh \to hh$ one; $P_{IJ}(s)$, the $\gamma\gamma \to \omega\omega$ ones (Eqs. (38a) and (38b)) that we newly incorporate in the unitarization in this work; and $R_J(s)$, the $\gamma\gamma \to hh$ (Eq. (38c)).

On the RC, the unitarity relations in Eq. (41), perturbative in α, can be split into three blocks, the Eqs. (53)–(55) that follow; first, those for the imaginary parts of the elastic amplitudes,

$$\text{Im}\, A_{0J} = |A_{0J}|^2 + |M_J|^2, \tag{53a}$$
$$\text{Im}\, A_{2J} = |A_{2J}|^2, \tag{53b}$$
$$\text{Im}\, M_J = A_{0J} M_J^* + M_J T_J^*, \tag{53c}$$
$$\text{Im}\, T_J = |M_J|^2 + |T_J|^2, \tag{53d}$$

which need to be solved as a coupled-channel problem with all channels being presumably strong. Only then is the solution fed to the second block for the $\gamma\gamma$ couplings, as we work to LO in α,

$$\text{Im}\, P_{0J} = P_{0J} A_{0J}^* + R_J M_J^*, \tag{54a}$$
$$\text{Im}\, R_J = P_{0J} M_J^* + R_J T_J^*. \tag{54b}$$

Finally, the isotensor block decouples from the isoscalar ones and becomes

$$\text{Im}\, A_{2J} = |A_{2J}|^2, \tag{55a}$$
$$\text{Im}\, P_{2J} = P_{2J} A_{2J}^*, \tag{55b}$$

which is identical to Eq. (42) and can be solved with the methods of Sect. 5.1, so we concentrate in what follows only in the first two blocks corresponding to isospin 0.

The previous discussion of Sect. 5.1 can be mimicked easily also for $I = 0$ by writing down first a reaction submatrix for the strongly interacting subchannel ${}_sF(\omega\omega, hh \to \omega\omega, hh)$,

$${}_sF = \begin{pmatrix} A_{00} & M_0 \\ M_0 & T_0 \end{pmatrix} \equiv \begin{pmatrix} A & M \\ M & T \end{pmatrix}, \tag{56}$$

a definition that can analogously be adopted for the matrices in the low-s chiral expansion, ${}_sF^{(0)}$ and ${}_sF^{(1)}$.

We now need to distinguish the cases $J = 0$ and $J = 2$ and handle the first right away. The matricial generalization of the IAM method in Eq. (45) yields a unitary ${}_s\tilde{F}$, from knowledge of the first two terms in the chiral expansion,

$${}_s\tilde{F} = {}_sF^{(0)}({}_sF^{(0)} - {}_sF^{(1)})^{-1}\, {}_sF^{(0)}. \tag{57}$$

The matrix elements of the IAM subreaction matrix can be likewise denoted with a tilde,

$${}_s\tilde{F} = \begin{pmatrix} \tilde{A} & \tilde{M} \\ \tilde{M} & \tilde{T} \end{pmatrix}. \tag{58}$$

This IAM approximation to the exact ${}_sF$ in Eq. (56) has all relevant properties: unitarity in the RC, i.e. $\text{Im}_s\, \tilde{F} = {}_s\tilde{F} \cdot_s \tilde{F}^\dagger =_s \tilde{F}^\dagger \cdot_s \tilde{F}$, analyticity, and matching to the HEFT chiral expansion at NLO.

If we also shorten notation $(P, R) \equiv (P_{00}, R_0)$, then from Eq. (53),

$$\text{Im} \begin{pmatrix} P \\ R \end{pmatrix} = {}_sF^* \cdot \begin{pmatrix} P \\ R \end{pmatrix}. \tag{59}$$

This is solved by the unitarized amplitude generalizing Eq. (46),

$$\begin{pmatrix} \tilde{P} \\ \tilde{R} \end{pmatrix} \equiv {}_s\tilde{F}({}_sF^{(0)})^{-1} \begin{pmatrix} P^{(0)} \\ R^{(0)} \end{pmatrix}. \tag{60}$$

Using the low-energy expansion ${}_s\tilde{F} = {}_sF^{(0)} + {}_sF^{(1)} + \cdots$, Eq. (60) turns into

$$\begin{aligned} \begin{pmatrix} \tilde{P} \\ \tilde{R} \end{pmatrix} &\equiv \tilde{F}(F^{(0)})^{-1} \begin{pmatrix} P^{(0)} \\ R^{(0)} \end{pmatrix} \\ &= (F^{(0)} + F^{(1)} + \ldots)(F^{(0)})^{-1} \begin{pmatrix} P^{(0)} \\ R^{(0)} \end{pmatrix} \\ &= \begin{pmatrix} P^{(0)} \\ R^{(0)} \end{pmatrix} + F^{(1)}(F^{(0)})^{-1} \begin{pmatrix} P^{(0)} \\ R^{(0)} \end{pmatrix} + \cdots. \end{aligned} \tag{61}$$

Note that Eqs. (38a)–(38c) explicitly show the perturbative order

$$\begin{pmatrix} P^{(0)} \\ R^{(0)} \end{pmatrix} \sim \begin{pmatrix} \mathcal{O}\left(\frac{s}{v^2}\right) + \mathcal{O}(\alpha) \\ \mathcal{O}(\alpha) \end{pmatrix}, \tag{62}$$

which excludes intermediate 2-photon states. Higher order contributions in s coming from the WBGBs and h rescatterings are taken into account in the IAM. For example, in expanding to one more order in Eq. (61) we find

$$F^{(1)}(F^{(0)})^{-1} \begin{pmatrix} P^{(0)} \\ R^{(0)} \end{pmatrix} \sim \begin{pmatrix} \mathcal{O}\left(\frac{s^2}{v^4}\right) + \mathcal{O}(\alpha) \\ \mathcal{O}\left(\frac{s}{v^2}\right) + \mathcal{O}(\alpha) \end{pmatrix}, \tag{63}$$

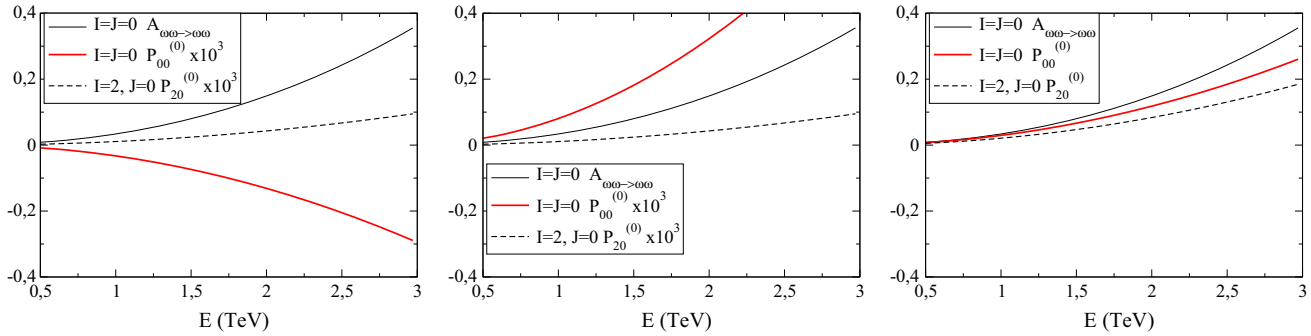

Fig. 2 Perturbative $\omega\omega \to \gamma\gamma$ amplitudes driven by the elastic $A(\omega\omega \to \omega\omega)$ shown as the thin line and equal on all plots for reference (corresponding to $a = 0.95$). *Left* The coupling to the $\gamma\gamma$ sector is produced only by α. *Center* Setting also $c_\gamma = 0.5/(16\pi^2)$ but $a_1 = a_2 = a_3 = 0$. *Right* $c_\gamma = 0 = a_1, a_3 - a_2 = 0.3$. Note that in the first two plots the P amplitudes have been multiplied by a factor 10^3 for visibility; not so in the third plot

as required. Equation (60) may be explicitly spelled out as

$$\tilde{P} = P^{(0)} \frac{\tilde{A}T^{(0)} - \tilde{M}M^{(0)}}{A^{(0)}T^{(0)} - (M^{(0)})^2} + R^{(0)} \frac{-\tilde{A}M^{(0)} + \tilde{M}A^{(0)}}{A^{(0)}T^{(0)} - (M^{(0)})^2}, \tag{64a}$$

$$\tilde{R} = P^{(0)} \frac{\tilde{M}T^{(0)} - \tilde{T}M^{(0)}}{A^{(0)}T^{(0)} - (M^{(0)})^2} + R^{(0)} \frac{\tilde{T}A^{(0)} - \tilde{M}M^{(0)}}{A^{(0)}T^{(0)} - (M^{(0)})^2}, \tag{64b}$$

in terms of the $IJ = 00$ IAM $\tilde{A}$, $\tilde{M}$ and $\tilde{T}$ partial-wave amplitudes of Eq. (58).

Finally, for $J = 2$ we find once more that the IAM method cannot be constructed without knowledge of the NNLO (in s) amplitude, so that the N/D coupled-channel method is used instead for the unitarization of the WBGBs and h scattering matrix elements (A_{I2}, M_2 and T_2). The matricial N/D formula, analogous to the elastic case of Eq. (49), is

$${}_s\tilde{F} = \left[1 + \frac{1}{2}G(s)F_L(-s)\right]^{-1} F_L(s), \tag{65}$$

where

$$G(s) = \frac{1}{\pi}\left[B(\mu)D^{-1} + \log\frac{-s}{\mu^2}\right], \tag{66a}$$

$$F_L(s) = \left[B(\mu)D^{-1} + \log\frac{s}{\mu^2}\right] Ds^2 = \pi G(-s) Ds^2, \tag{66b}$$

are the matricial versions of Eq. (50a) and following. Note that, although we are in the coupled-channel case in the sense that $\omega\omega \to hh \to \omega\omega$ rescattering takes place, hh states do not couple with $\gamma\gamma$ for $J = 2$ [see Eq. (26)]. Thus, we need the matricial N/D method of Eq. (65) for unitarizing the $\omega\omega \to \omega\omega$ partial waves, but the coupling with $\gamma\gamma$ states can be computed by using the (scalar) equation (51).

Finally, for the purpose of cross-checking the IAM in the $J = 0$ case, the P_{02} matrix elements can be estimated via the coupled-channel N/D by a matrix analogous of Eq. (51),

$$\tilde{P}_{I2} = {}_s\tilde{F}_{I2}\left(F_{\mathrm{L},I2}\right)^{-1} P^{(0)}_{I2}, \quad I = 0, 2, \tag{67}$$

with $\tilde{P}_{I2}$ a column vector of two components $\tilde{P}$, $\tilde{R}$.

6 Some numerical examples

We start by commenting on the perturbative partial-wave amplitudes very briefly. Referring to Eq. (38), we see that the NLO perturbative amplitudes $P^{(0)}_{02}$, $P^{(0)}_{22}$ and $R^{(0)}_0$ are all constant, so we do not plot them. The two $P^{(0)}$ amplitudes coming from the isoscalar $\omega\omega$ state, quadratic in energy, are shown in Fig. 2. Therein and in what follows we have taken $\alpha_{\mathrm{EM}}(Q^2 = 0) = \frac{1}{137}$ as the emitted photons are real. From the parameters of the EWSBS, we have taken all NLO coefficients to zero, and $b = a^2$, so that the only slight separation from the SM is driven by $a = 0.95$; the further parameters of the photon sector are indicated in the figure.

All the amplitudes shown in the figure display the expected quadratic growth with energy (linearity in s). Eventually they must violate the unitarity bounds, for example by $|A_{00}| > 1$, which occurs already below 3 TeV if we increase $1 - a$ or other parameters of the HEFT.

The first two plots show P amplitudes that are much smaller than the elastic A amplitude, as demanded by the smallness of α. On the contrary, the third plot exposes values of P of the same order of those of A. This means that the a priori counting of Sect. 2.1 fails for the value of $(a_1 - a_2 + a_3)$ chosen around 0.3; this maximum value, still allowed by previous empirical constraints, is too large in comparison to the "natural" values of the a_i, of order 10^{-3}. We do not employ such large values again later.

The approach that we have developed can be used to describe resonances that could be found in experimental data from the LHC and relate different channels. Figure 3 shows

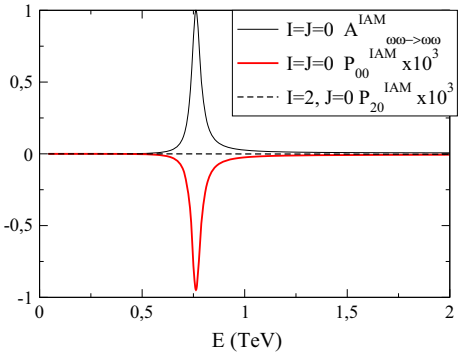

Fig. 3 With $a = 0.81$, $b = a^2$, $a_5(\mu = 0.75\ \text{TeV}) = 0.0023$ and other NLO parameters at that scale set to zero, the IAM accommodates a narrow resonance in the scalar channel. We show the imaginary part of the elastic amplitude and the imaginary part of the scalar photon amplitudes (multiplied by 10^3 as in Fig. 2)

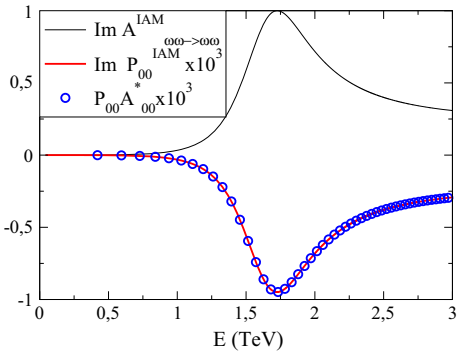

Fig. 4 Example of the broad resonance generated by elastic $\omega\omega$ scattering, which illustrates the unitarity of P_{00} in the absence of coupling to the hh channel. The parameters employed are $a = 0.81$, $b = a^2$, $a_4(\mu = 3\ \text{TeV}) = 4 \times 10^{-4}$. (All other NLO parameters vanish at that scale)

a narrow resonance, with $\Gamma/M \sim 0.06$. This is useful to make contact with the large body of theoretical work following the $\gamma\gamma$ statistical fluctuation in the CMS and ATLAS data (we next proceed to more phenomenologically viable resonances).

Although the electromagnetic interactions do not conserve weak isospin, our choice of P_{00} and P_{20} amplitudes implies that only the first is fed by a scalar resonance in the $\omega\omega$ channel, as is patent in the figure.

The signs of the imaginary parts of P_{00} and A_{00} are seen to be opposite. This is a consequence of $a^2 - 1 < 0$ for the choice $a = 0.81$ and Eqs. (12a), (14a) and (46).

Next, we provide an example of a typical broad resonance in Fig. 4.

Once more, the only non-vanishing parameter for the two-photon sector is $\alpha = 1/137$. The imaginary part of P_{00} (note it has again been multiplied by 10^3) presents a clear resonating shape driven by that of A. We also show how well the unitarity relation of Eq. (42) is satisfied by our numerical

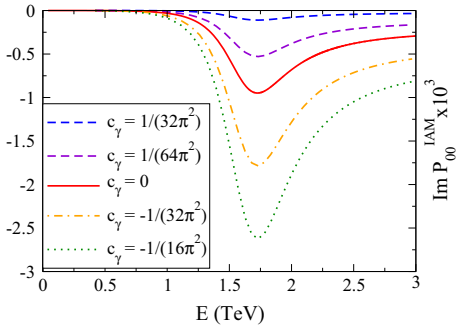

Fig. 5 Dependence of P_{00} on c_γ

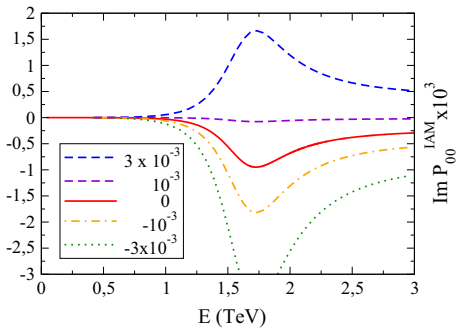

Fig. 6 Dependence of the P_{00} amplitude from Fig. 4 on $(a_1 - a_2 + a_3)$ (values thereof are given in the legend)

program: the IAM is indeed up to the task, with unitarity satisfied exactly in s and to first order in α.

In Fig. 5 we show the dependence of P_{00} on the parameter c_γ within its allowed 2σ band. The solid line corresponds to $c_\gamma = 0$. Positive values thereof diminish the intensity of P_{00}, negative values increase it. While the line shape of the resonance is also affected by the value of c_γ, the position of the maximum (controlled by the IAM $\omega\omega$ amplitude) is not.

In turn, Fig. 6 shows the dependence on values of the $(a_1 - a_2 + a_3)$ parameter combination that are way smaller (of order $\sim 10^{-3}$) than the maximum allowed by the 2σ bounds (as argued above, values of order 0.1 are unnaturally large and overturn the counting that we follow). Once more, while the position of the pole is the same for all curves, the line shape and especially the total normalization of the curve do depend on this a_i parameter combination.

We now move on to a coupled-channel example, illustrated in Fig. 7. As $a^2 - b$ increases, the hh channel is coupled with larger LO strength. This makes the resonance of Fig. 3, which we take to exemplify the point, broader and somewhat less intense in the $\gamma\gamma$ channel, resembling more and more the coupled-channel resonance described in [48].

An interesting feature is that the resonance moves toward higher energies. To understand it, we note that the pole of the IAM amplitude (with $a^2 - b$ set to 0) comes from a denominator $\frac{1}{A^{(0)} - A^{(1)}}$. Upon activating the hh channel coupling

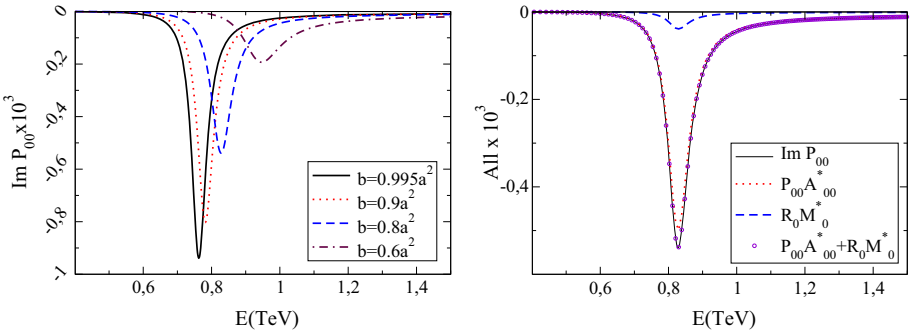

Fig. 7 *Left* The resonance of Fig. 3 is coupled to the hh with the strength $(b - a^2)$ indicated in the legend for each line, the other parameters remaining the same as earlier. *Right* Test of the unitarity relation in Eq. (54) for the case $b = 0.8a^2$

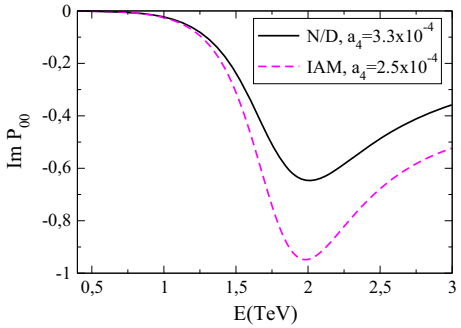

Fig. 8 Comparison of the IAM and N/D methods. The LO parameters are $a = 0.81$, $b \simeq a^2$; the only non-vanishing NLO parameter at $\mu = 3$ TeV is a_4 as indicated for each of the two lines

with $a^2 - b$, the matrix amplitude in Eq. (57) has as denominator, in view of $T^{(0)} = 0$, a slightly more complicated one, $\frac{1}{A^{(0)} - A^{(1)} + \frac{(M^{(0)} - M^{(1)})^2}{T^{(1)}}}$. The last term can shift the zeros of the denominator, and thus the resonance position, according to the sign of $T^{(1)}$. The leading $(a^2 - b)^2$ factor cancels in the ratio, so the effect is not huge, but there remains sensitivity to the next order, $(a^2 - b)^3$ from the $M^{(0)} M^{(1)}$ cross product. Both $A^{(0)}$ and $\mathrm{Re}T^{(1)}$ happen to be positive [33], so that $\mathrm{Re}(\frac{(M^{(0)} - M^{(1)})^2}{T^{(1)}})$ has the same sign as $A^{(0)}$ and reinforces it. Thus, $A^{(1)}$ has to be larger to obtain a cancellation, and this requires a higher s, whence the resonance increases in energy.

The right panel of the same figure then serves to demonstrate unitarity as per the first of Eq. (54). We see in the plot how elastic unitarity according to Eq. (42) fails, and how the addition of the $R_0 M_0^*$ component is precisely what achieves coupled-channel unitarity.

Figure 8 permits a comparison of the IAM and N/D methods in a case where both are applicable, the scalar–isoscalar channel. We have taken b very close a^2 to avoid the coupled-channel complication here (already shown to work in Fig. 7). With both methods we have varied a_4 until a scalar resonance appears at 2 TeV. The necessary value of this parameter is somewhat different, by 25%. The width and the minimum value of the P_{00} amplitude are not identical either (which could be perhaps arranged by varying some of the other NLO parameters, but we do not see the need at this stage). In conclusion, while both methods give qualitative similar results, their comparison gives us a warning that there is a systematic uncertainty in the choice of unitarization scheme of order one part in four.

Finally, in Fig. 9 we show P_{02}, the $\gamma\gamma$ amplitude with the initial $\omega\omega$ in the isoscalar-tensor channel. The left plot is dedicated to showing a nonresonant tensor amplitude; for ease of comparison, we employ the same parameters as produced a scalar resonance in Fig. 4. An interesting remark is that at relatively low energies the ratio between the photon production amplitude and the elastic $\omega\omega$ one, P_{02}/A_{02}, is much more sizable than its scalar counterpart P_{00}/A_{00}. This comes about because in Eq. (38a) there is an electromagnetic α coupling as in all the photon amplitudes, but it is constant (s independent) as opposed to A_{02}, which has an Adler zero at $s = 0$. Therefore, both amplitudes can be shown in the same plot by enhancing the photon one only by a factor 10^2, whereas in the scalar case we have been employing a factor 10^3.

As for the right plot of Fig. 9, we have increased a_4 (from 4×10^{-4} in the left plot to 3×10^{-3}) so a tensor resonance appears below 3 TeV. The resonance is clearly visible, in the same position, in the $\gamma\gamma \to \omega\omega$ P_{02} amplitude as in the elastic amplitude. (The latter is only two orders of magnitude larger, as just discussed). Coupled-channel unitarity is also clearly demonstrated as $\mathrm{Im}\, P_{02} = P_{02} A_{02}^*$.

Many more example calculations are interesting, but we content ourselves with these examples until experimental data shows whether there is merit in pursuing further computations, and specifically which ones.

7 Conclusions

In this article we have coupled the EWSBS described with HEFT (for $E < 4\pi v \sim 3$ TeV) and the equivalence theorem (for energies $E > M_h,\ M_W$), in the regime of unitarity saturation and resonances, to the two-photon channel, which is a promising detection avenue for new physics.

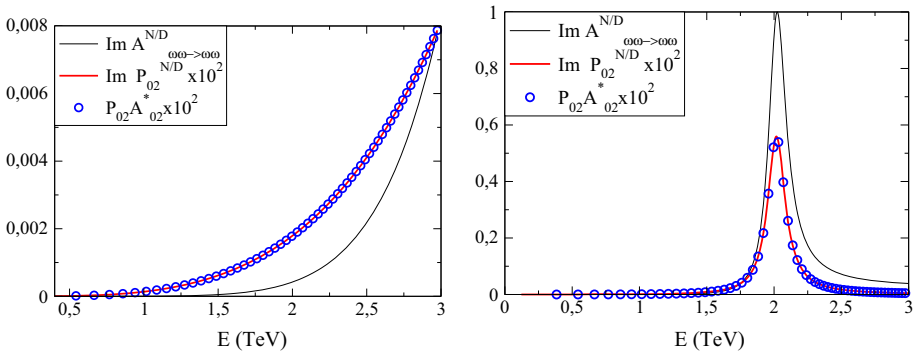

Fig. 9 P_{02} isoscalar, tensor amplitude in the N/D method. *Left* Same parameters as in Fig. 4. *Right* We increase $a_4 = 3 \times 10^{-3}$ to induce a tensor resonance in the elastic $\omega\omega$ amplitude that is neatly reproduced in the photon–photon amplitude. In both cases we test unitarity

We have developed the necessary unitarization formalism with two different, well explored methods (IAM and N/D), that are equivalent (up to NNLO) to the NLO perturbative amplitudes of [42] at low energies but that, unlike those of the HEFT, can be employed to describe any resonances of the EWSBS.

For example, in Figs. 3 and 4 we have shown that both a light, narrow, and a heavier, broader resonance feeding the $\gamma\gamma$ spectrum can be parametrized in this approach, in terms of a, a_4 and a_5, which control the EWSBS. What the production cross section is for those particular resonances is work of phenomenological interest that we postpone to imminent work within an expanded collaboration.

Our formalism assumes that the symmetry-breaking dynamics in the W, Z and h sector is stronger than their electromagnetic coupling to γs. Nevertheless we have also considered the NLO counterterms that arise in coupling $\gamma\gamma$ to the EWSBS. As long as their values remain "natural", our counting in Fig. 1 suggests that perturbation theory is valid in coupling $\gamma\gamma$, and that the resonating $\omega\omega$ (and/or hh) amplitudes can be separately computed first. Our theory satisfies Watson's final-state theorem in that the phases of the photon–photon production amplitude coincide with those of the elastic EWSBS amplitudes.

A technical challenge that we have overcome is that of projecting the (earlier known) Feynman amplitudes into $\gamma\gamma$-helicity amplitudes of definite total angular momentum J and stemming from $\omega\omega$ states of definite custodial isospin I. This was necessary and convenient as any resonance or new particle produced in the custodially invariant EWSBS sector will have specific I, J but the detection in the $\gamma\gamma$ channel loses memory of I; a complete set of observables, however, includes the photon helicities λ_1 and λ_2 (though for many cross-section calculations one may sum them).

Even in the absence of new resonances, the set of projected amplitudes that we have provided can be useful to parametrize separations from the SM in a relatively low-energy regime below 3 TeV, where the partial-wave series converges quickly.

We are currently collaborating with other authors in the preparation of a document with simple estimates for collider cross-sections of typical resonances as seen in the two-photon channel.

Finally, another natural final-state channel that couples with sufficient intensity to the EWSBS, and that may serve as an LHC probe thereof, is the $t\bar{t}$ one. We are separately exploring it with the same methods and have recently shown that within HEFT this channel coupling admits a perturbative expansion in powers of $M_t/\sqrt{s}$, obtaining the unitarized amplitudes needed for its description in the resonance region [62]. The calculation follows lines analogous to those here presented.

Acknowledgements We thank for useful conversation and suggestions J.J. Sanz-Cillero, D. Espriu, and M.J. Herrero. Work supported by Spanish MINECO Grants FPA2011-27853-C02-01, FPA2014-53375-C2-1-P and BES-2012-056054 (RLD).

Funded by SCOAP[3].

References

1. G. Aad et al. (ATLAS Collaboration), Phys. Lett. B **716**, 1 (2012)
2. S. Chatrchyan et al. (CMS Collaboration), Phys. Lett. B **716**, 30 (2012)
3. G. Aad et al. (ATLAS Collaboration), Phys. Lett. B **726**, 88 (2013) [Erratum: Phys. Lett. B **734**, 406 (2014)]
4. S. Chatrchyan et al. (CMS Collaboration), JHEP **1306**, 081 (2013)
5. R. Alonso, E.E. Jenkins, A.V. Manohar, Phys. Lett. B **754**, 335 (2016)
6. R. Alonso, M.B. Gavela, L. Merlo, S. Rigolin, J. Yepes, Phys. Lett. B **722**, 330 (2013) [Erratum: Phys. Lett. B **726**, 926 (2013)]
7. R. Alonso, M.B. Gavela, L. Merlo, S. Rigolin, J. Yepes, Phys. Rev. D **87**(5), 055019 (2013)
8. M.B. Gavela, K. Kanshin, P.A.N. Machado, S. Saa, JHEP **1503**, 043 (2015)
9. M.B. Gavela, J. Gonzalez-Fraile, M.C. Gonzalez-Garcia, L. Merlo, S. Rigolin, J. Yepes, JHEP **1410**, 044 (2014)

10. A. Pich, I. Rosell, J.J. Sanz-Cillero, EPJ Web Conf. **60**, 19009 (2013)
11. G. Buchalla, O. Catà, C. Krause, Nucl. Phys. B **880**, 552 (2014) [Note that this and other articles by the same authors employ the exponential parametrization of the Goldstone bosons whereas we use the spherical one; both are equivalent as shown in [29] in the $\gamma\gamma$ context]
12. G. Buchalla, O. Cata, A. Celis, C. Krause, Eur. Phys. J. C **76**(5), 233 (2016)
13. F. Feruglio, Int. J. Mod. Phys. A **8**, 4937 (1993)
14. R. Contino, C. Grojean, M. Moretti, F. Piccinini, R. Rattazzi, JHEP **1005**, 089 (2010). doi:10.1007/JHEP05(2010)089. arXiv:1002.1011 [hep-ph]
15. The 4th CERN Yellow Report gives further detail and applications *in extenso*, see D. de Florian et al. (LHC Higgs Cross Section Working Group Collaboration), Handbook of LHC Higgs cross sections: 4. Deciphering the nature of the Higgs sector. arXiv:1610.07922 [hep-ph]
16. T. Appelquist, C. Bernard, Phys. Rev. D **22**, 200 (1980)
17. A. Longhitano, Phys. Rev. D **22**, 1166 (1980)
18. A. Longhitano, Nucl. Phys. B **188**, 118 (1981)
19. A. Dobado, D. Espriu, M.J. Herrero, Phys. Lett. B **255**, 405 (1991)
20. B. Holdom, J. Terning, Phys. Lett. B **247**, 88 (1990)
21. M. Golden, L. Randall, Nucl. Phys. B **361**, 3 (1991)
22. I. Brivio, J. Gonzalez-Fraile, M.C. Gonzalez-Garcia, L. Merlo, Eur. Phys. J. C **76**(7), 416 (2016)
23. J.M. Cornwall, D.N. Levin, G. Tiktopoulos, Phys. Rev. D **10**, 1145 (1974)
24. C.E. Vayonakis, Lett. Nuovo Cim. **17**, 383 (1976)
25. B.W. Lee, C. Quigg, H. Thacker, Phys. Rev. D **16**, 1519 (1977)
26. M.S. Chanowitz, M.K. Gaillard, Nucl. Phys. **261**, 379 (1985)
27. M.S. Chanowitz, M. Golden, H. Georgi, Phys. Rev. D **36**, 1490 (1987)
28. A. Dobado, J.R. Peláez, Nucl. Phys. B **425**, 110 (1994)
29. A. Dobado, J.R. Peláez, Phys. Lett. B **329**, 469 (1994) [Addendum: Phys. Lett. B **335**, 554 (1994)]
30. H.J. He, Y.P. Kuang, X.Y. Li, Phys. Lett. B **329**, 278 (1994)
31. R.L. Delgado, A. Dobado, F.J. Llanes-Estrada, JHEP **1402**, 121 (2014)
32. R.L. Delgado, A. Dobado, F.J. Llanes-Estrada, J. Phys. G **41**, 025002 (2014)
33. R.L. Delgado, A. Dobado, F.J. Llanes-Estrada, Phys. Rev. D **91**(7), 075017 (2015)
34. T.N. Truong, Phys. Rev. Lett. **61**, 2526 (1988)
35. A. Dobado, M.J. Herrero, T.N. Truong, Phys. Lett. B **235**, 134 (1990)
36. A. Dobado, M.J. Herrero, T.N. Truong, Phys. Lett. B **235**, 129 (1990)
37. C.N. Yang, Phys. Rev. **77**, 242 (1950)
38. A. Manohar, P. Nason, G.P. Salam, G. Zanderighi, How bright is the proton? A precise determination of the photon parton distribution function. Phys. Rev. Lett. **117**(24), 242002 (2016)
39. V. Khachatryan et al. (CMS Collaboration), JHEP **1608**, 119 (2016). arXiv:1604.04464 [hep-ex]. doi:10.1007/JHEP08(2016)119
40. V.I. Telnov, Nucl. Part. Phys. Proc. **273–275**, 219 (2016)
41. J. Gronberg, Rev. Accel. Sci. Tech. **7**, 161 (2014)
42. R.L. Delgado, A. Dobado, M.J. Herrero, J.J. Sanz-Cillero, JHEP **1407**, 149 (2014)
43. K. Agashe, R. Contino, A. Pomarol, Nucl. Phys. B **719**, 165 (2005)
44. R. Contino, L. Da Rold, A. Pomarol, Phys. Rev. D **75**, 055014 (2007)
45. D. Barducci et al., JHEP **1309**, 047 (2013)
46. E. Halyo, Mod. Phys. Lett. A **8**, 275 (1993)
47. W.D. Goldberger, B. Grinstein, W. Skiba, Phys. Rev. Lett. **100**, 111802 (2008)
48. R.L. Delgado, A. Dobado, F.J. Llanes-Estrada, Phys. Rev. Lett. **114**(22), 221803 (2015)
49. V. Khachatryan et al. (CMS Collaboration), Eur. Phys. J. C **75**(5), 212 (2015)
50. The ATLAS Collaboration (ATLAS Collaboration), ATLAS-CONF-2014-009
51. P.P. Giardino, Aspects of LHC phenomenology, PhD Thesis (2013), Università di Pisa
52. J. Bijnens, F. Cornet, Two Pion Production in Photon-Photon Collisions, Nucl. Phys. B **296** (1988) 557
53. M. Fabbrichesi, M. Pinamonti, A. Tonero, A. Urbano, Phys. Rev. D **93**(1), 015004 (2016)
54. M.E. Rose, *Elementary Theory of Angular Momentum* (Wiley, New York, 1957)
55. S.U. Chung, CERN-71-08, BNL-QGS-02-0900, doi:10.5170/CERN-1971-008. https://suchung.web.cern.ch/suchung/spinfm1.pdf
56. J.A. Aguilar Saavedra, *Helicity Formalism and Applications* (Godel Impresiones Digitales, Granada, 2015)
57. L.D. Landau, V.B. Berestetskii, E.M. Lifshitz, L.P. Pitaevskii, *Relativistic Quantum Theory*, vol. 4 (Wesley, Reading, 1971)
58. D. Espriu, F. Mescia, B. Yencho, Phys. Rev. D **88**, 055002 (2013)
59. D. Espriu, B. Yencho, Phys. Rev. D **87**, 055017 (2013)
60. D. Espriu, F. Mescia, Phys. Rev. D **90**(1), 015035 (2014)
61. T. Corbett, O.J.P. Éboli, M.C. Gonzalez-Garcia, Phys. Rev. D **93**(1), 015005 (2016)
62. A. Castillo, R.L. Delgado, A. Dobado, F.J. Llanes-Estrada, arXiv:1607.01158 [hep-ph]